Inhibition of Influenza A Virus Infection *in Vitro* by Saliphenylhalamide-Loaded Porous Silicon Nanoparticles

Luis M. Bimbo,[†] Oxana V. Denisova,[‡] Ermei Mäkilä,[†,§] Martti Kaasalainen,[§] Jef K. De Brabander,[⊥] Jouni Hirvonen,[†] Jarno Salonen,[§] Laura Kakkola,[‡] Denis Kainov,[‡,∥] and Hélder A. Santos[†,*]

[†]Division of Pharmaceutical Technology, Faculty of Pharmacy, University of Helsinki, FI-00014, Finland, [‡]Institute for Molecular Medicine Finland (FIMM), University of Helsinki, FI-00014, Finland, [§]Laboratory of Industrial Physics, Department of Physics and Astronomy, University of Turku, FI-20014, Finland, [⊥]Department, of Biochemistry, University of Texas Southwestern Medical Center, Dallas, Texas 75390-9038, United States, and [∥]Siauliai University, 76285, Lithuania

ABSTRACT Influenza A viruses (IAVs) cause recurrent epidemics in humans, with serious threat of lethal worldwide pandemics. The occurrence of antiviral-resistant virus strains and the emergence of highly pathogenic influenza viruses have triggered an urgent need to develop new anti-IAV treatments. One compound found to inhibit IAV, and other virus infections, is saliphenylhalamide (SaliPhe). SaliPhe targets host vacuolar-ATPase and inhibits acidification of endosomes, a process needed for productive virus infection. The major obstacle for the further development of SaliPhe as antiviral drug has been its poor solubility. Here, we investigated the possibility to increase SaliPhe solubility by loading the compound in thermally hydrocarbonized porous silicon (THCPSi) nanoparticles. SaliPhe-loaded nanoparticles were further investigated for the ability to inhibit influenza A infection in human retinal pigment epithelium and Madin-Darby canine kidney cells, and we show that upon release from THCPSi, SaliPhe inhibited IAV infection *in vitro* and reduced the amount of progeny virus in IAV-infected cells. Overall, the PSi-based nanosystem exhibited increased dissolution of the investigated anti-IAV drug SaliPhe and displayed excellent *in vitro* stability, low cytotoxicity, and remarkable reduction of viral load in the absence of organic solvents. This proof-of-principle study indicates that PSi nanoparticles could be used for efficient delivery of antivirals to infected cells.

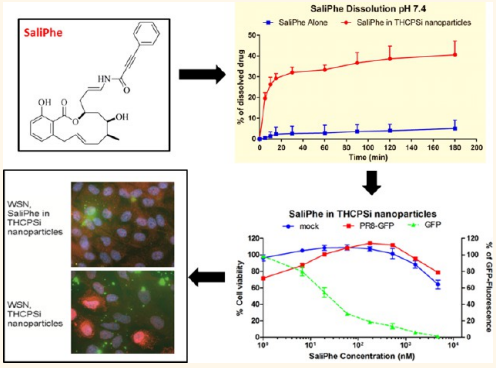

KEYWORDS: porous silicon · nanoparticle · influenza A · saliphenylhalamide · drug delivery · inhibition · virus

Influenza viruses cause annual epidemics of respiratory infections that are associated with significant morbidity and mortality and high economic costs. For example, in the U.S. it is estimated that the cost to the economy of seasonal influenza epidemics is in the range of $71−167 billion.[1] Mutations and reassortment of genomic segments between strains and subtypes enable new viruses to emerge by acquiring new properties including the development of resistance to existing virus-targeted antiviral drugs.[2]

Human influenza A viruses (IAVs) invade the respiratory tract causing acute respiratory infections, with occasional ocular infection. The IAVs replicate in lung dendritic cells, type II pneumocytes, and alveolar macrophages as well as in retinal epithelial cells.[3−5] Vaccinations and antiviral therapeutics have not stopped the emergence and rapid spread of seasonal H3N2, pandemic H1N1, and potentially pandemic H7N9 viruses, which represent a major threat to public health. This has emphasized the urgent need to develop efficient antiviral strategies.[6,7] Due to their high mutation rate, these viruses acquire resistance to available virus-directed drugs. Small molecules that target host functions implicated in virus infection could therefore be more efficient against IAV infection.[5]

In order to ensure the efficient production of viral particles, IAVs rely on the subversion of cellular functions, *e.g.*, endocytosis, transcription, translation, and apoptosis.[8] Thus, the disruption of the cellular functions

* Address correspondence to helder.santos@helsinki.fi.

Received for review April 24, 2013 and accepted July 26, 2013.

Published online July 26, 2013
10.1021/nn402062f

normally implicated in IAV infection represents an attractive strategy to inhibit IAV infection, diminishing the risk of developing viral resistance.[9] Recently, several small molecules have been shown to display a potent inhibitory effect on IAV infection and have provided novel insights into IAV−host cell interaction.[5] One of these compounds is saliphenylhalamide (SaliPhe), a drug proved to be an effective anti-IAV agent by inhibiting vacuolar ATPase (v-ATPase) activity and preventing the acidification of endosomes, thus arresting the IAVs in the endocytic compartments.[2,5,9,10] SaliPhe inhibits infection of noncancerous human cells with different IAV strains that are resistant to available antiviral drugs (oseltamivir and amantadine). SaliPhe also increased survival rates of mice infected with lethal doses of mouse-adapted IAV strain.[2] Importantly, this small molecule also inhibited infection with other viruses that represent a serious threat to human health (*e.g.*, influenza B, Bunyamwera and Sindbis viruses).[5] However, SaliPhe has low water solubility, and this has been a significant bottleneck for the successful translation of this compound into the clinic.[2]

The leveraging of nanotechnology-based carrier systems for antiviral therapy can help surmount the poor SaliPhe water solubility, reduce side-effects of antiviral compounds, and increase drug bioavailability.[11] In particular, porous silicon (PSi) is an excellent nanoengineered material that encompasses several advantageous properties for drug delivery and imaging.[12−17] This material offers distinctive advantages when compared with other materials such as its top-down production method[18] and easy surface modification for different purposes such as stabilization[19] and imaging.[12,20,21] In addition to its biocompatibility,[22,23] PSi materials have been found to increase the dissolution of otherwise poorly water-soluble drugs loaded within its mesopores.[22,24] Furthermore, water-soluble molecules and vulnerable molecules such as peptides[25−27]and small interfering RNA[28] have also been successfully loaded in and released from PSi particles. The PSi-based particles were also found to be straightforwardly customizable to adapt to the harsh conditions of the stomach and intestinal lumen,[29−31] improving their cytocompatibility,[32] or even to modulate plasma protein adsorption,[33] which renders them ideal vehicles for drug delivery purposes.

Here, we developed a method to obtain SaliPhe-loaded thermally hydrocarbonized PSi (THCPSi) nanoparticles and assessed their potential to inhibit IAV infection *in vitro*. The SaliPhe-loaded THCPSi nanoparticles were thoroughly characterized and were found to rescue the human retinal pigment epithelium (RPE) and Madin-Darby canine kidney (MDCK) cells from viral infection at noncytotoxic concentrations. Furthermore, fluorescence microscopy showed that the SaliPhe-loaded PSi nanoparticles inhibited viral infection by preventing the nuclear accumulation of viral ribonuclear proteins. Importantly, the particles allowed the delivery of SaliPhe in the absence of dimethyl sulfoxide (DMSO), and they increased the drug dissolution rates compared to the pure drug. To our knowledge, this is the first demonstration of the potential of PSi nanoparticles to deliver anti-IAV drugs to IAV-infected cells and to inhibit the infection.

RESULTS AND DISCUSSION

Preparation and Characterization of THCPSi Nanoparticles. The PSi films were produced by electrochemical etching of Si-wafers with HF and ethanol, and the nanoparticles were prepared from the PSi films as described elsewhere.[23] The THCPSi nanoparticles used in this study had a *Z*-average diameter of 129 ± 10 nm and a polydispersity index (PDI) of 0.112, with a pore diameter of 10.7 ± 0.3 nm, specific surface area of 210 ± 15 m^2/g, and pore volume of 0.56 ± 0.03 cm^3/g. The measured zeta (ζ)-potential of the THCPSi nanoparticles was −43 mV. Figure 1a shows a transmission electron microscope (TEM) picture of the THCPSi nanoparticles. These nanoparticles show a spherical-round shape, with no evidence of aggregates. In the dynamic light scattering (DLS) measurements, the size distribution was found to be narrow and the polydispersion of all nanoparticles was below 0.2, indicating highly monodisperse nanoparticles (Figure 1b). The measured ζ-potential also indicates a rather negatively charged surface, which prevents aggregation and stabilizes the particles in suspension.

The loading degree of SaliPhe in the mesopores of THCPSi nanoparticles is mainly dependent on the interactions of the drug compound and the PSi matrix. At the appropriate pH, PSi spontaneously adsorbs positively charged molecules.[34] SaliPhe was loaded into the THCPSi nanoparticles using dichloromethane and ethanol (see Materials and Methods section). The loading degree of SaliPhe into THCPSi nanoparticles was of 2.88 ± 0.11 wt % determined by HPLC, which can be attributed to the drug's high log P (6.63 ± 0.63; theoretical calculations using ACD/Laboratories Software V11.02) and chemical structure (Figure 2). Nonetheless, the loading degree was sufficient to attain a therapeutic effect on the RPE and MDCK cells infected with IAV as described below.

Enhanced SaliPhe Release Rate from THCPSi Nanoparticles. After characterizing empty THCPSi nanoparticles and SaliPhe-loaded THCPSi nanoparticles, the drug releasing properties of the nanoparticles were investigated. SaliPhe is a sparingly water-soluble compound (6.2×10^{-7} mol/L in nonbuffered water, pH 6.9; theoretical calculations using ACD/Laboratories Software V11.02), which is one of the major problems for administering this drug.[2] At pH 7.4, it was observed that the THCPSi nanoparticles released *ca.* 30% of the loaded SaliPhe during the first 15 min, but afterward a less

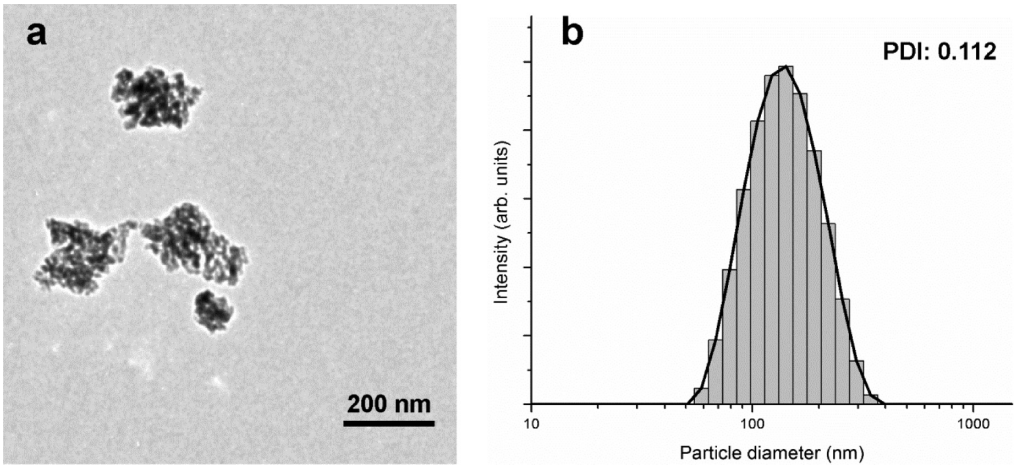

Figure 1. TEM image of THCPSi nanoparticles (a) used in this study and their respective size distribution by DLS (b). Scale bar is 200 nm.

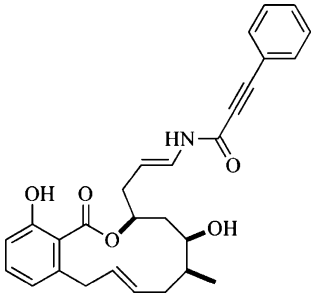

Figure 2. Chemical structure of SaliPhe.

pronounced, yet gradual release of the drug was attained (Figure 3a). Conversely, the pure form of SaliPhe could reach only approximately 5% dissolution within the same time period and in the same conditions as the SaliPhe-loaded THCPSi nanoparticles. Furthermore, the SaliPhe release from the THCPSi nanoparticles in Dulbecco's minimal essential medium (DMEM), media used in cell experiments, showed a similar profile to the SaliPhe alone, reaching around 11% of dissolution and the SaliPhe loaded inside the THCPSi nanoparticles reaching around 40% (Figure 3b). In addition, the total amount of SaliPhe released during the course of the experiment was quantified at 24 and 48 h and was 45.8% and 47.4%, respectively, which represents about 3.52 and 3.64 μg of SaliPhe per 267 μg of THCPSi nanoparticles, respectively. It has been hypothesized that the increased dissolution rate of drugs loaded inside the pores of PSi is due to their confinement and inability to crystallize inside the pores, leading to a lower Gibbs free energy state of the drug (disordered) and subsequent increase in drug dissolution behavior.[35] The dissolution of the PSi matrix itself, which increases with time at alkaline pH and a temperatures of 37 °C, can also be used as an advantage for releasing the loaded drug.[36] The continuous release of the drug in the amorphous state from the THCPSi nanoparticles can lead not only to an increase in the dissolution rate but also to a sustained release profile of compounds from the matrix[26] that could maintain the therapeutic levels of the compound for a longer period of time, being potentially beneficial for antiviral compounds to achieve a lasting effect during the desired therapeutic window.

Cytotoxicity and Antiviral Efficacy of the SaliPhe-Loaded THCPSi Nanoparticles. SaliPhe dissolved in DMSO, SaliPhe-loaded THCPSi nanoparticles, and empty THCPSi nanoparticles were assessed for their cytotoxicity and virus inhibition properties in human RPE cells. Cells were either mock infected or infected with IAV strain A/PR8-NS116-GFP (PR8-GFP), which upon infection expresses GFP-protein in fusion with viral nonstructural (NS1) protein. PR8-GFP-infected RPE cells also die upon infection, and thus, both cell viability and GFP fluorescence were measured at 48 h postinfection (hpi). As shown in Figure 4, cells infected with PR8-GFP and treated with increasing concentrations of SaliPhe in DMSO showed a decrease in the GFP fluorescence and an increase in cell viability, indicating that SaliPhe in DMSO blocks the virus infection and rescues cells from virus-induced death. However, a remarkable decrease in the cell viability of noninfected cells was observed, particularly at the higher doses of the drug, indicating that SaliPhe in DMSO is cytotoxic (Figure 4a). As expected, in the absence of any inhibitor, the empty THCPSi nanoparticles did not promote a decrease in GFP fluorescence nor rescued the infected cells. The empty particles, however, did not show any cytotoxicity toward the RPE cells (Figure 4b). Importantly, the SaliPhe-loaded THCPSi nanoparticles substantially decreased the GFP fluorescence in the PR8-GFP-infected cells and rescued them from virus-induced cell death. Furthermore, the SaliPhe-loaded THCPSi nanoparticles induced only approximately 20% cytotoxicity compared to approximately 80% with SaliPhe in DMSO, with the highest concentration (5 μM) of compound in the PR8-GFP-infected cells (Figure 4c).

The SaliPhe dissolved in DMSO, SaliPhe-loaded THCPSi nanoparticles, and empty THCPSi nanoparticles

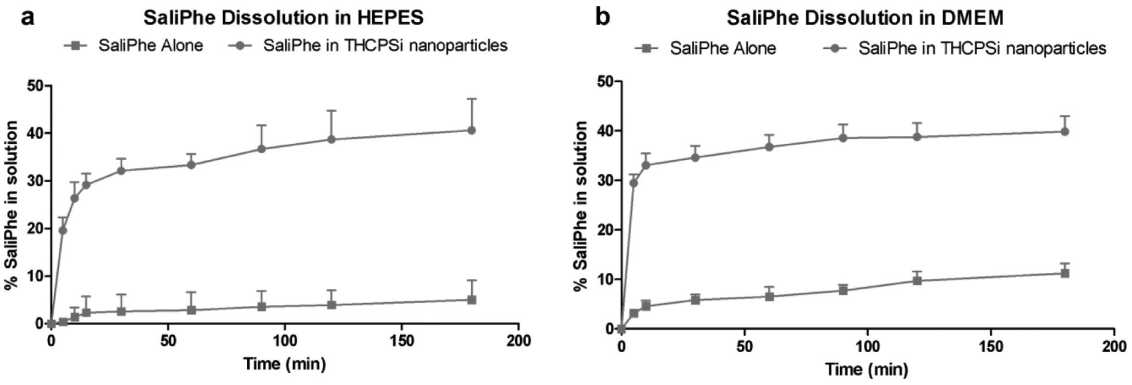

Figure 3. Dissolution profiles of SaliPhe alone (■) and SaliPhe-loaded THCPSi nanoparticles (●) in (a) buffer solution (pH 7.4) at 37 °C and (b) DMEM (pH 7.4). Error bars represent mean ± SD ($n \geq 3$).

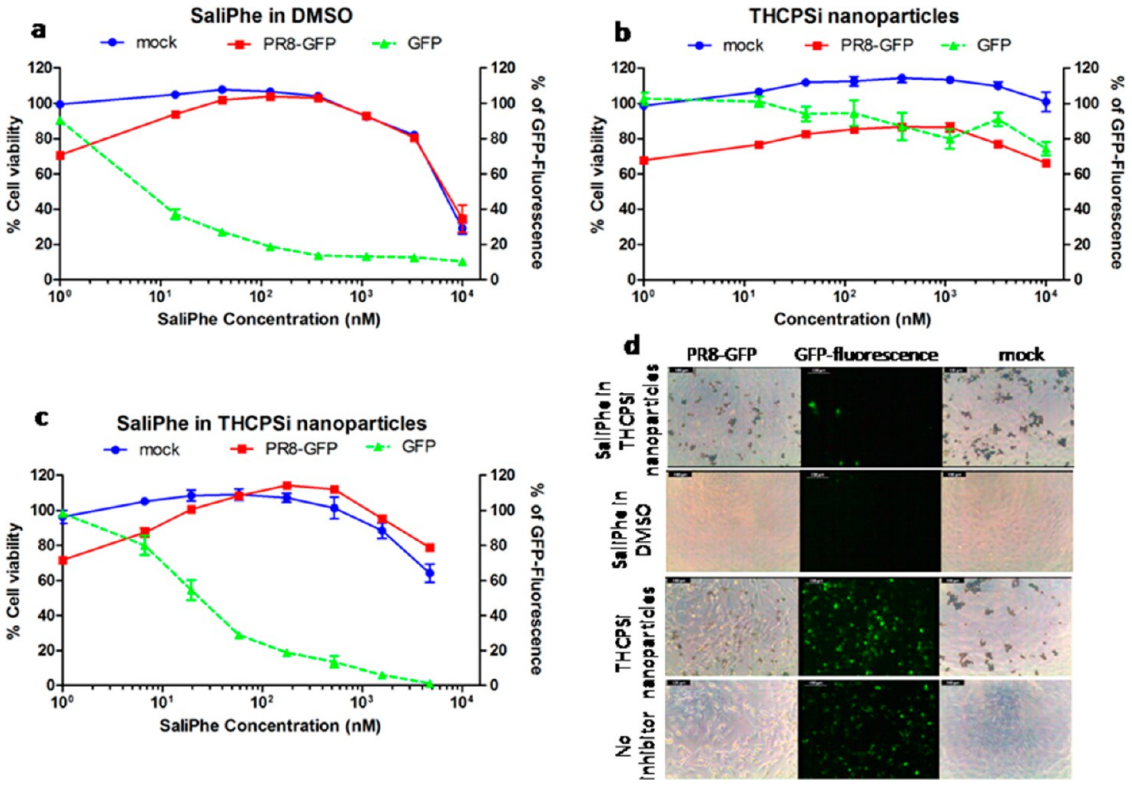

Figure 4. RPE cell viability and PR8-GFP virus inhibition by (a) SaliPhe dissolved in DMSO, (b) empty THCPSi nanoparticles, and (c) SaliPhe-loaded THCPSi nanoparticles assessed in terms of GFP expression (fluorescence) and cell viability in mock infected and PR8-GFP virus infected cells. Error bars represent mean ± SD ($n \geq 3$). (d) Fluorescence and light microscopy images of mock infected and PR8-GFP virus infected RPE cells treated with 1 μM SaliPhe-loaded THCPSi nanoparticles, SaliPhe in DMSO, and empty THCPSi nanoparticles. Scale bars are 200 μm.

were further assessed for cytotoxicity and virus inhibition properties in a widely used cell model for IAV infection, in MDCK cells. Cells were mock infected or infected with PR8-GFP, and the cell viability and GFP fluorescence were measured at 24 hpi. As shown in Figure 5, increasing concentrations of SaliPhe in DMSO inhibited virus infection (a decrease in GFP fluorescence and an increase in cell viability were observed), but as with RPE cells, SaliPhe in DMSO was cytotoxic at concentrations above 0.5 μM (Figure 5a). The empty THCPSi nanoparticles did not rescue infected cells, and they did not show cytotoxicity, not even at the highest concentration (Figure 5b). Importantly, the SaliPhe-loaded THCPSi nanoparticles promoted cell viability and reduced GFP fluorescence without eliciting cytotoxic response in concentrations up to 1 μM. The cytotoxicity observed above 1 μM is most likely due to the drug's inherent toxicity at high concentrations (Figure 5c).

Due to the different sensitivity of the two cell lines to IAV infection and their equal tolerance for the THCPSi nanoparticles, the SaliPhe-loaded THCPSi nanoparticles promoted a more pronounced rescue of the PR8-GFP infected MDCK (about 40% viability at 1 nM to 95% viability at 0.5 μM) compared with RPE cells

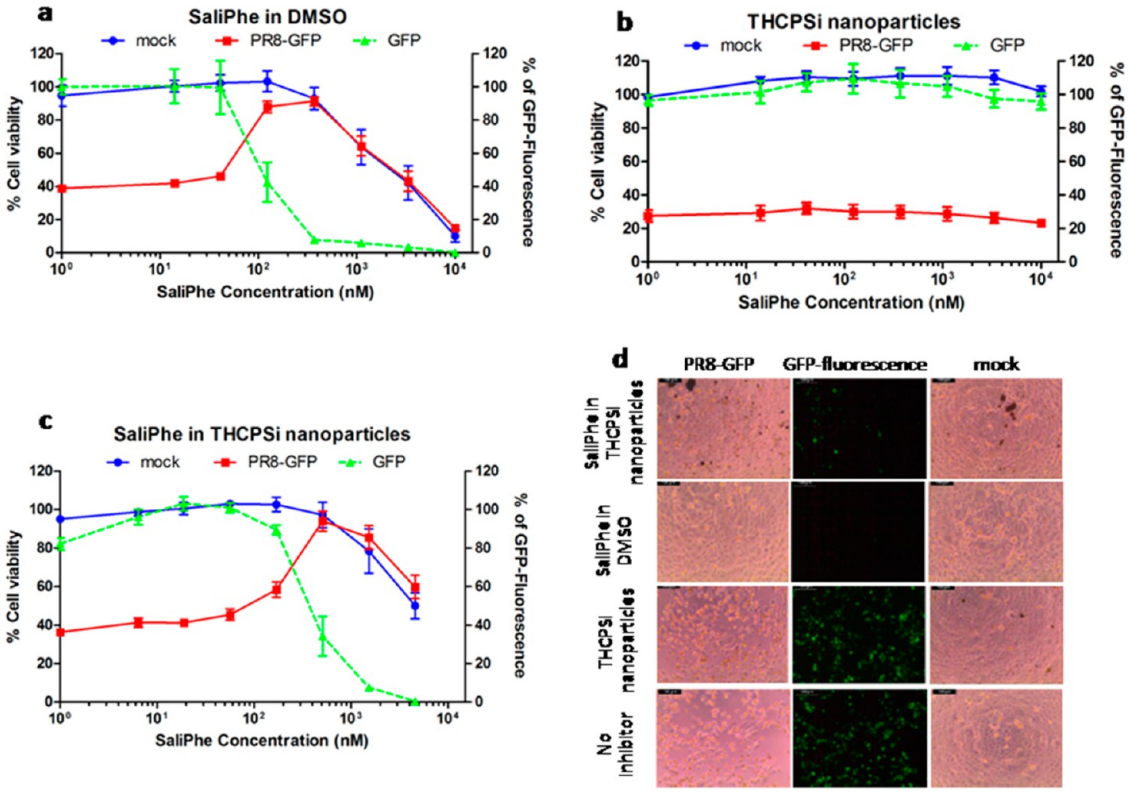

Figure 5. MDCK cell viability and PR8-GFP virus inhibition by (a) SaliPhe dissolved in DMSO, (b) empty THCPSi nanoparticles, and (c) SaliPhe-loaded THCPSi nanoparticles assessed in terms of GFP expression (fluorescence) and cell viability in mock infected and PR8-GFP virus infected cells. Error bars represent mean ± SD ($n \geq 3$). (d) Fluorescence and light microscopy images of mock infected and PR8-GFP infected MDCK cells and treated with 1 μM SaliPhe-loaded THCPSi nanoparticles, SaliPhe dissolved in DMSO, and empty THCPSi nanoparticles. Scale bars are 200 μm.

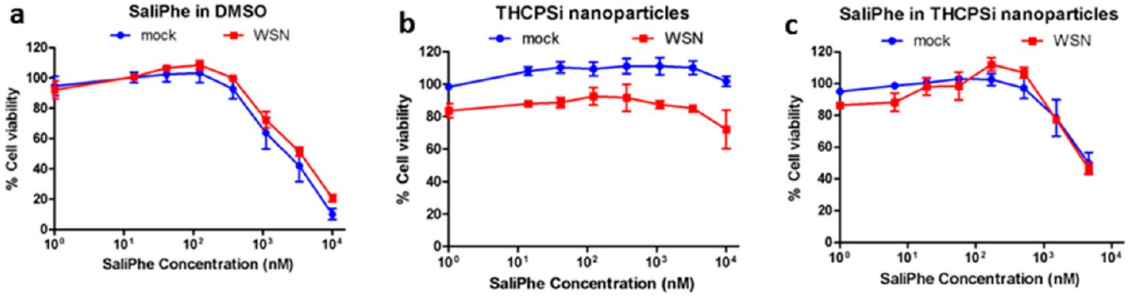

Figure 6. Cell viability of mock infected (blue) or WSN-infected (red) MDCK cells treated with (a) SaliPhe dissolved in DMSO, (b) empty THCPSi nanoparticles, and (c) SaliPhe-loaded THCPSi nanoparticles. Error bars represent mean ± SD ($n \geq 3$).

(which had about 70% viability at 1 nM to 100% viability at 0.02 μM) (Figures 4 and 5).

Overall, the therapeutic window for SaliPhe in MDCK cells (if we consider viabilities over 50% and GFP expression below 10%) was between 370 and 1111 nM for SaliPhe dissolved in DMSO and between 169 and 4581 nM for SaliPhe loaded in THCPSi nanoparticles. In RPE cells, none of the concentrations tested of SaliPhe dissolved in DMSO could achieve a reduction of GFP fluorescence below 10%, whereas the SaliPhe loaded in THCPSi nanoparticles could reduce the GFP fluorescence below 10% in concentrations ranging from 1579 to 4738 nM, while keeping the viability well above 50%. This wider therapeutic window is therefore an important feature that supports THCPSi nanoparticles as excellent carriers for SaliPhe and is able to circumvent and control the inherent toxicity of the drug at concentrations above 1 μM.

PR8-GFP virus encodes GFP protein fused to a NS1 protein, potentially affecting the virus–cell interactions. Thereby the antiviral efficacy of SaliPhe-loaded THCPSi nanoparticles was also tested for wild-type IAV strain, A/WSN/33 (WSN), which encodes intact viral proteins. MDCK cells were mock infected or infected with WSN, and the cell viability was measured at 24 hpi. Cells infected with WSN and treated with the SaliPhe dissolved in DMSO showed recovery from infection at concentrations up to 0.3 μM, with a subsequent steep

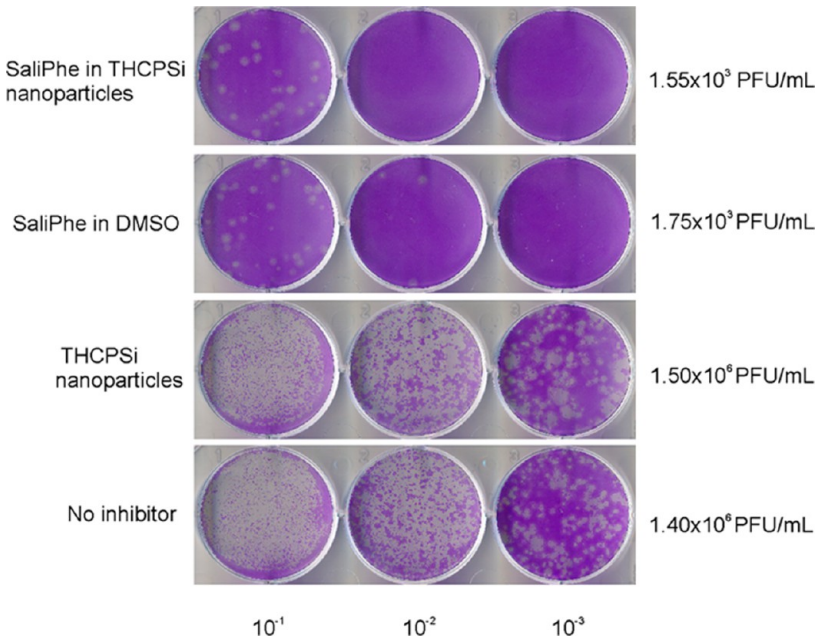

Figure 7. Virus titers measured with a plaque assay. Representative plaque assays are shown for PR8-GFP-infected MDCK cells 24 hpi in the absence of inhibitor and in the presence of empty THCPSi nanoparticles, 1 μM SaliPhe dissolved in DMSO, and 1 μM SaliPhe loaded in THCPSi nanoparticles. The number of plaques (clear spots) observed in 10-fold dilutions represents the amount of virus (*i.e.*, virus titer) in a given dilution. PFU corresponds to plaque forming units.

decline in cell viability as the concentration of the drug increased (Figure 6a). The empty THCPSi nanoparticles did not show any cytotoxicity and did not affect the virus infection (Figure 6b). With the SaliPhe-loaded THCPSi nanoparticles, MDCK cells were rescued from IAV infection with the onset of toxicity appearing at a later concentration (Figure 6c) than with the DMSO-dissolved SaliPhe, for example, at 70% viability with 1 μM SaliPhe in DMSO *vs* 1.5 μM THCPSi-loaded SaliPhe.

Effect of SaliPhe-Loaded Nanoparticles on Viral Titers. In addition to blockage of infection, it is important to verify that the applied drug also decreases the viral titers, *i.e.*, affects the amount of progeny virions produced by infected cells. To verify that SaliPhe-loaded THCPSi nanoparticles also reduce the virus titers, MDCK cells were either mock infected or infected with PR8-GFP virus, and the amount of newly produced viruses was measured with a plaque assay. Figure 7 shows the degree of inhibition mediated by empty THCPSi nanoparticles, SaliPhe dissolved in DMSO, and SaliPhe-loaded THCPSi nanoparticles. Treatment of PR8-GFP-infected MDCK cells with SaliPhe, both in DMSO and loaded into the THCPSi nanoparticles, resulted in significant 2 log reduction in virus titers as compared to controls (no inhibitor and empty nanoparticles). This further confirmed the potential anti-IAV effect of SaliPhe-loaded THCPSi nanoparticles as a possible substitute system for SaliPhe dissolved in DMSO. Thus, SaliPhe-loaded THCPSi nanoparticles are foreseen as a promising platform to deliver antiviral compounds and to reduce the viral load in the absence of highly cytotoxic organic solvents.

Immunofluorescence Analysis of the Infected and THCPSi Nanoparticle-Treated Cells. Upon infection, IAV is taken up in endosomes to the cells by endocytosis. Viral nucleoprotein (NP) complexes are released from the acidified endosomes and transported to the nucleus. Also newly synthesized proteins forming RNPs accumulate into the nucleus prior to the assembly of new virions.[10] The release of viral RNP complexes from the endosomes is triggered by the low pH of the late endosomes.[37,38] Therefore, an inhibition of the acidification of the endosomes can prevent IAV entry.[2] The main mechanism of SaliPhe for preventing IAV infection is thought to be the blocking of v-ATPase activity,[2] inhibiting acidification of endosomes, and, thus, arresting IAV entry.

To visualize that SaliPhe-loaded THCPSi nanoparticles block the IAV infection before nuclear accumulation of RNPs, RPE cells were either mock infected or infected with WSN, and the localization of viral NP was visualized at 18 hpi with immunofluorescence. In addition, to visualize the localization of the THCPSi nanoparticles, the particles were tagged with a fluorochrome, FITC. As shown in Figure 8, in RPE cells infected with WSN and treated with empty THCPSi nanoparticles (in green), the NPs (in red) accumulated in the nuclei. In cells infected with WSN and treated with SaliPhe-loaded THCPSi nanoparticles (0.5 μM), the accumulation of viral NPs into nuclei was blocked. In Figure 8 it is also apparent that some of the THCPSi nanoparticles (in green) accumulated in the intracellular compartments of the cells, most probably in the endosomes. This internalization of the THCPSi can

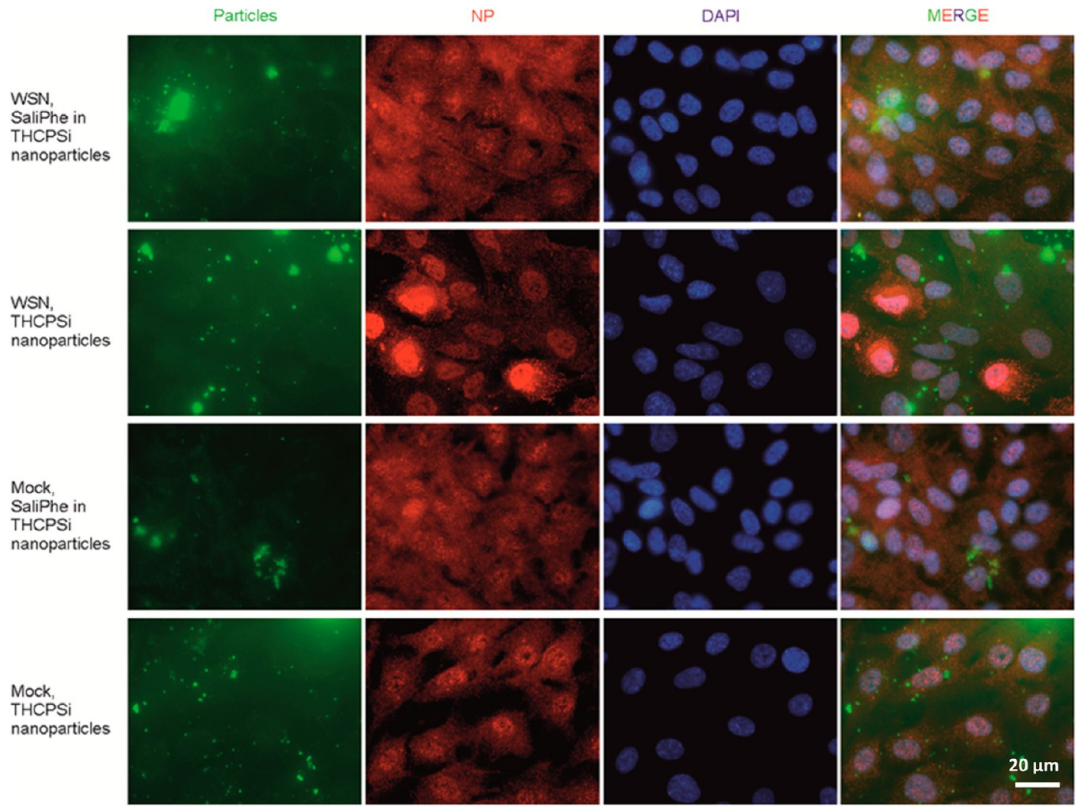

Figure 8. Fluorescence microscopy images of mock and WSN-infected RPE cells treated with 0.5 μM SaliPhe-loaded THCPSi nanoparticles and empty THCPSi nanoparticles. The nuclei of the cells were stained with DAPI (blue), the THCPSi nanoparticles were tagged with an FITC label (green), and the viral NP was detected with antibody (red). Scale bar is 20 μm.

potentially explain the more pronounced anti-IAV effect (Figures 4 to 6), resulting from the ability of SaliPhe to prevent the acidification of endosomes, thus arresting the IAVs in the endocytic compartments.[2,5,9] These results verify that SaliPhe loaded in and released from THCPSi nanoparticles has the same activity as SaliPhe dissolved in DMSO and is also able to block IAV infection at the early steps of virus life cycle.

CONCLUSION

One of the great public health challenges nowadays is the potential emergence of highly pathogenic influenza strains, such as avian H5N1 and H7N9, and new pandemic strains, such as A/H1N1/pdm09. Due to the inability or inadequacy of the current therapies to prevent and cure IAV infections, alternative therapies for IAV infection are required. However, the poor water solubility and toxicity of potential antiviral drugs is a big problem in drug development. Here, we overcame this by loading water-insoluble SaliPhe into THCPSi nanoparticles, which allowed steady release of SaliPhe in inorganic solvents without any loss of activity or change in the physicochemical properties of the compound. Moreover, SaliPhe-loaded THCPSi nanoparticles rescued cells from IAV infection at noncytotoxic concentrations. Interestingly, the therapeutic window was wider in comparison with SaliPhe dissolved in DMSO. Thereby the THCPSi nanoparticles are an excellent carrier for SaliPhe and are able to circumvent and control the inherent toxicity of the drug at concentrations above 1 μM. Overall, SaliPhe-loaded THCPSi nanoparticles exhibit low cytotoxicity and remarkable reduction of viral titers in the absence of organic solvents. This is the first proof-of-principle that shows the potential of PSi nanoparticles to deliver SaliPhe to cells and to inhibit IAV infection. Further optimization of the delivery routes, such as inhalation or intravenous injection, is currently envisioned, and further preclinical evaluation is warranted for the development of PSi nanosystems as a potential platform for the targeted delivery of antiviral compounds *in vivo*.

MATERIALS AND METHODS

Preparation of THCPSi Nanoparticles. Free-standing PSi multilayer films were anodized using single-crystal Si wafers ⟨100⟩ of p^+-type with resistivity values of 0.01−0.02 Ωcm. The anodization was done using a 1:1 (v/v) hydrofluoric acid (HF, 38%)−ethanol electrolyte. The multilayer structure was anodized using an etching profile with alternating low and high current density pulses.[23] The hydrocarbonization treatment to obtain surface

stabilization consisted in exposing the particles to a 1:1 (v/v) flow of N_2 and acetylene for 15 min at room temperature, followed by 15 min at 500 °C, and then cooling to room temperature under N_2 flush, as described previously.[14,30] Wet ball milling was used to reduce the size of the hydrocarbonized PSi multilayer films, while the surface oxidation was minimized by using 1-decene as the milling liquid.[23] The final size separation and exchange of the suspension media were done by centrifugation.

Particle Characterization. The THCPSi nanoparticles were characterized by conducting N_2 sorption measurements at 77 K (Tristar 3000, Micromeritics Inc., GA, USA). The specific surface area was calculated using the Brunauer–Emmett–Teller (BET) theory, whereas the total pore volume was obtained from the total adsorbed amount at a relative pressure $p/p_0 = 0.97$ (Figure S1). The average pore diameter was calculated using the obtained surface area and pore volume, assuming the pores to be cylindrical. In order to investigate the morphology of the THCPSi nanoparticles, TEM images were taken from a TEM (FEI Tecnai, F12, Philips Electron Optics, The Netherlands). The samples for TEM were prepared by adding droplets of the THCPSi nanoparticle suspensions on coated copper grids and allowing them to dry for ca. 24 h prior to measurements. DLS for size distribution and ζ-potential measurements were made on a ZetaSizer Nano instrument (Malvern Ltd., UK) in ultrapure water.

Loading of THCPSi Nanoparticles with SaliPhe. SaliPhe was synthesized as described elsewhere.[9] A stock of 10 mM SaliPhe in 100% DMSO was prepared and stored at −80 °C before use. SaliPhe was loaded into the THCPSi nanoparticles by dissolving 2 mg of the drug in 200 μL of dichloromethane and then adding 800 μL of pure ethanol to the solution. The solution was incubated at 40 °C at 200 mbar for 1 h. This is simply to concentrate the SaliPhe in the solution for the loading and at the same time prevent drug crystallization by using both low pressure and temperature. The resulting solution was incubated with 1 mg of THCPSi nanoparticles for 1 h under stirring for the loading. Subsequently, the nanoparticles were centrifuged at 8000 rpm for 2 min, and the supernatant was discarded. In order to determine the drug loading degree, a fraction of the SaliPhe-loaded THCPSi nanoparticles (200 μg) was dispersed in 2 mL of absolute ethanol for 2 h and then centrifuged at 13 200 rpm for 5 min. The supernatant was collected and analyzed using a Thermo Separation Products (TSP) HPLC comprising a TSP degasser, Spectra System P4000 pump, a Spectra System AS3000 autosampler, a Spectra System UV6000LP, a UV/vis lamp, a Spectra System 4000 diode array detector, and the software ChromQuest 4.2. The particles were then reincubated with absolute ethanol for a further 24 and 48 h in order to quantify the residual SaliPhe in the THCPSi nanoparticles. The loading degree of SaliPhe in the THCPSi nanoparticles was determined by the mass ratio (μg) of compound per 100 μg of THCPSi nanoparticles.

***In Vitro* Drug Release Studies.** In order to assess the drug release from the THCPSi nanoparticles, 267 μg of SaliPhe-loaded THCPSi nanoparticles or the equivalent amount of pure SaliPhe (around 7.69 μg of loaded SaliPhe) was dispersed in 4 mL of HEPES-buffered saline or DMEM, pH 7.4, and shaken at 175 rev/min. One milliliter aliquots were taken at 5, 10, 15, 30, 60, 90, 120, and 180 min and centrifuged at 13 200 rpm for 2 min, and supernatants were collected for the HPLC analysis as described above. After each aliquot was taken, 1 mL of fresh medium was added to replace the volume taken to keep the volume constant. All assays were made in triplicate.

Cells and Viruses. MDCK cells were maintained in DMEM supplemented with 10% fetal bovine serum (FBS), 2 mM L-glutamine, and 50 U/mL penicillin–streptomycin mix (PenStrep). Human hTERT-immortalized retinal pigment epithelial cells were maintained in DMEM/Nutrient F-12 HAM (DMEM-F12) containing 2 mM L-glutamine, 10% FBS, 50 U/mL PenStrep, and 0.348% $NaHCO_3$. All cells were grown at 37 °C and 5% CO_2. The IAV strains A/WSN/33 (WSN; H1N1) and A/PR8-NS116-GFP (PR8-GFP; H1N1) were propagated in MDCK cells and monkey Vero-E6 cells, respectively. Virus stocks were titrated by a plaque assay on MDCK cells.

***In Vitro* Virus Infections and Compound Efficacy Testing.** The SaliPhe efficacy testing was done in 96-well plates in RPE or MDCK cells. Typically, 40 000 cells were seeded in 100 μL of appropriate cell growth medium and grown for 24 h. The growth medium was changed to a virus growth medium (VGM) containing 0.2% bovine serum albumin (BSA), 2 mM L-glutamine, 50 U/mL PenStrep, and 1 μg/mL L-1-tosylamido-2-phenylethyl chloromethyl ketone trypsin (TPCK)-trypsin in DMEM or DMEM-F12 with 0.348% $NaHCO_3$. SaliPhe dissolved in DMSO was added to the cells in 3-fold serial dilutions at seven different concentrations starting from 10 μM. THCPSi nanoparticles loaded with SaliPhe were added to the cells with equivalent drug concentrations as the pure drug dissolved in DMSO, taking into consideration the 2.88 wt % loading degree of the drug in the THCPSi nanoparticles. The empty THCPSi nanoparticles were added in equivalent amount to loaded THCPSi nanoparticles. The cells were infected with viruses (PR8-GFP or WSN) at a multiplicity of infection (MOI) of 3 or mock infected. The cell viability was measured using the Cell TiterGlo assay (Promega). Luminescence and GFP fluorescence were read with a PHERAstar FS plate reader (BMG Labtech).

Virus Titration. The efficacy of the SaliPhe-loaded THCPSi nanoparticles was further validated using plaque assays. The cells were treated with the SaliPhe dissolved in DMSO and with SaliPhe-loaded THCPSi nanoparticles at noncytotoxic concentrations and infected with PR8-GFP (MOI 0.1). Supernatants were collected at 24 hpi. The supernatants were 10-fold diluted in DMEM-based VGM and added to MDCK cells on 6-well plates. After 1 h the cells were overlaid with medium containing 1.2% Avicel, 0.2% BSA, 50 units/mL PenStrep, 2 mM L-glutamine, and 1 μg/mL TPCK-trypsin in minimal essential medium and incubated for 2 days. The cells were fixed with 4% paraformaldehyde in phosphate buffer solution (PBS) and stained with 0.1% crystal violet in 1% methanol, 20% pure ethanol, and 3.6% formaldehyde. Virus titers were determined by calculating plaque forming units (PFU) (clear spots) for sample dilutions and expressed as PFU/mL for the sample.

Immunofluorescence. RPE cells were grown on cover glasses in 6-well plates, treated with FITC-tagged THCPSi nanoparticles or 0.5 μM SaliPhe-loaded FITC-tagged THCPSi nanoparticles, and infected with WSN at MOI 3. At 18 hpi cells were fixed with 4% paraformaldehyde (in PBS) for 20 min at room temperature. PBS with 1% BSA and 0.1% Triton X-100 was used for blocking and permeabilization of the fixed cells and for dilution of antibodies. Nucleoprotein of WSN virus was detected with rabbit polyclonal antibody (1:1000, from Ilkka Julkunen, Finland); the secondary antibody was Alexa Fluor 594 labeled goat anti-rabbit IgG (H+L) (1:1000, Invitrogen). Nuclei were counterstained with DAPI. Images were captured with a Nikon 90i microscope and processed with NIS Elements AR software.

Conflict of Interest: The authors declare no competing financial interest.

Acknowledgment. L.M.B. acknowledges the Finnish Cultural Foundation for financial support. O.V.D., D.K., and L.K. acknowledge the Jane and Aatos Erkko Foundation, the Centre for International Mobility (CIMO), and the Academy of Finland (decision numbers 138644 and 255852) for financial support. D.K. acknowledges also grant no. VP1-3.1-ŠMM-07-K-03-069. J.K.D.B. acknowledges support from the Robert A. Welch Foundation (grant I-1422) and is the holder of the Julie and Louis Beecherl, Jr., Chair in Medical Science. H.A.S. acknowledges the Academy of Finland (decision numbers 252215 and 256394), the University of Helsinki, and the European Research Council under the European Union's Seventh Framework Programme (FP/2007-2013) grant no. 310892 for financial support.

Supporting Information Available: Nitrogen adsorption–desorption isotherms. This material is available free of charge *via* the Internet at http://pubs.acs.org.

REFERENCES AND NOTES

1. Graham-Rowe, D. Racing against the Flu. *Nature* **2011**, *480*, S2–S3.
2. Müller, K. H.; Kainov, D. E.; El Bakkouri, K.; Saelens, X.; De Brabander, J. K.; Kittel, C.; Samm, E.; Müller, C. P. The Proton Translocation Domain of Cellular Vacuolar Atpase Provides a Target for the Treatment of Influenza A Virus Infections. *Br. J. Pharmacol.* **2011**, *164*, 344–357.
3. Weinheimer, V. K.; Becher, A.; Tonnies, M.; Holland, G.; Knepper, J.; Bauer, T. T.; Schneider, P.; Neudecker, J.;

Ruckert, J. C.; Szymanski, K.; *et al*. Influenza A Viruses Target Type II Pneumocytes in the Human Lung. *J. Infect. Dis.* **2012**, *206*, 1685–1694.
4. Gu, J.; Xie, Z.; Gao, Z.; Liu, J.; Korteweg, C.; Ye, J.; Lau, L. T.; Lu, J.; Zhang, B.; McNutt, M. A.; *et al*. H5N1 Infection of the Respiratory Tract and Beyond: A Molecular Pathology Study. *Lancet* **2007**, *370*, 1137–1145.
5. Denisova, O. V.; Kakkola, L.; Feng, L.; Stenman, J.; Nagaraj, A.; Lampe, J.; Yadav, B.; Aittokallio, T.; Kaukinen, P.; Ahola, T.; *et al*. Obatoclax, Saliphenylhalamide, and Gemcitabine Inhibit Influenza A Virus Infection. *J. Biol. Chem.* **2012**, *287*, 35324–35332.
6. de Jong, M. D.; Thanh, T. T.; Khanh, T. H.; Hien, V. M.; Smith, G. J. D.; Chau, N. V.; Cam, B. V.; Qui, P. T.; Ha, D. Q.; Guan, Y.; *et al*. Brief Report—Oseltamivir Resistance during Treatment of Influenza A (H5N1) Infection. *New Engl. J. Med.* **2005**, *353*, 2667–2672.
7. Lackenby, A.; Thompson, C. I.; Democratis, J. The Potential Impact of Neuraminidase Inhibitor Resistant Influenza. *Curr. Opin. Infect. Dis.* **2008**, *21*, 626–638.
8. Müller, K. H.; Kakkola, L.; Nagaraj, A. S.; Cheltsov, A. V.; Anastasina, M.; Kainov, D. E. Emerging Cellular Targets for Influenza Antiviral Agents. *Trends Pharmacol. Sci.* **2012**, *33*, 89–99.
9. Lebreton, S.; Jaunbergs, J.; Roth, M. G.; Ferguson, D. A.; De Brabander, J. K. Evaluating the Potential of Vacuolar ATPase Inhibitors as Anticancer Agents and Multigram Synthesis of the Potent Salicylihalamide Analog Saliphenylhalamide. *Bioorg. Med. Chem. Lett.* **2008**, *18*, 5879–5883.
10. Liu, S. L.; Zhang, Z. L.; Tian, Z. Q.; Zhao, H. S.; Liu, H.; Sun, E. Z.; Xiao, G. F.; Zhang, W.; Wang, H. Z.; Pang, D. W. Effectively and Efficiently Dissecting the Infection of Influenza Virus by Quantum-Dot-Based Single-Particle Tracking. *ACS Nano* **2012**, *6*, 141–150.
11. Lembo, D.; Cavalli, R. Nanoparticulate Delivery Systems for Antiviral Drugs. *Antivir. Chem. Chemother.* **2010**, *21*, 53–70.
12. Santos, H. A.; Bimbo, L. M.; Lehto, V. P.; Airaksinen, A. J.; Salonen, J.; Hirvonen, J. Multifunctional Porous Silicon for Therapeutic Drug Delivery and Imaging. *Curr. Drug Discov. Technol.* **2011**, *8*, 228–249.
13. Santos, H. A.; Bimbo, L. M.; Herranz, B.; Shahbazi, M.-A.; Hirvonen, J.; Salonen, J. Nanostructured Porous Silicon in Preclinical Imaging: Moving from Bench to Bedside. *J. Mater. Res.* **2013**, *28*, 152–164.
14. Salonen, J.; Kaukonen, A. M.; Hirvonen, J.; Lehto, V. P. Mesoporous Silicon in Drug Delivery Applications. *J. Pharm. Sci.* **2008**, *97*, 632–653.
15. Kinnari, P.; Mäkilä, E.; Heikkilä, T.; Salonen, J.; Hirvonen, J.; Santos, H. A. Comparison of Mesoporous Silicon and Non-Ordered Mesoporous Silica Materials as Drug Carriers for Itraconazole. *Int. J. Pharm.* **2011**, *414*, 148–156.
16. Vale, N.; Mäkilä, E.; Salonen, J.; Gomes, P.; Hirvonen, J.; Santos, H. A. New Times, New Trends for Ethionamide: *In Vitro* Evaluation of Drug-Loaded Thermally Carbonized Porous Silicon Microparticles. *Eur. J. Pharm. Biopharm.* **2012**, *81*, 314–323.
17. Tahvanainen, M.; Rotko, T.; Mäkilä, E.; Santos, H. A.; Neves, D.; Laaksonen, T.; Kallonen, A.; Hamalainen, K.; Peura, M.; Serimaa, R.; *et al*. Tablet Preformulations of Indomethacin-Loaded Mesoporous Silicon Microparticles. *Int. J. Pharm.* **2012**, *422*, 125–131.
18. Chiappini, C.; Tasciotti, E.; Fakhoury, J. R.; Fine, D.; Pullan, L.; Wang, Y. C.; Fu, L.; Liu, X.; Ferrari, M. Tailored Porous Silicon Microparticles: Fabrication and Properties. *ChemPhysChem* **2010**, *11*, 1029–1035.
19. Mäkilä, E.; Bimbo, L. M.; Kaasalainen, M.; Herranz, B.; Airaksinen, A. J.; Heinonen, M.; Kukk, E.; Hirvonen, J.; Santos, H. A.; Salonen, J. Amine Modification of Thermally Carbonized Porous Silicon with Silane Coupling Chemistry. *Langmuir* **2012**, *28*, 14045–14054.
20. Santos, H. A.; Salonen, J.; Bimbo, L. M.; Lehto, V. P.; Peltonen, L.; Hirvonen, J. Mesoporous Materials as Controlled Drug Delivery Formulations. *J. Drug Deliv. Sci. Technol.* **2011**, *21*, 139–155.
21. Park, J. H.; Gu, L.; von Maltzahn, G.; Ruoslahti, E.; Bhatia, S. N.; Sailor, M. J. Biodegradable Luminescent Porous Silicon Nanoparticles for *in Vivo* Applications. *Nat. Mater.* **2009**, *8*, 331–336.
22. Bimbo, L. M.; Mäkilä, E.; Laaksonen, T.; Lehto, V. P.; Salonen, J.; Hirvonen, J.; Santos, H. A. Drug Permeation Across Intestinal Epithelial Cells Using Porous Silicon Nanoparticles. *Biomaterials* **2011**, *32*, 2625–2633.
23. Bimbo, L. M.; Sarparanta, M.; Santos, H. A.; Airaksinen, A. J.; Makila, E.; Laaksonen, T.; Peltonen, L.; Lehto, V. P.; Hirvonen, J.; Salonen, J. Biocompatibility of Thermally Hydrocarbonized Porous Silicon Nanoparticles and Their Biodistribution in Rats. *ACS Nano* **2010**, *4*, 3023–3032.
24. Salonen, J.; Laitinen, L.; Kaukonen, A. M.; Tuura, J.; Bjorkqvist, M.; Heikkilä, T.; Vaha-Heikkilä, K.; Hirvonen, J.; Lehto, V. P. Mesoporous Silicon Microparticles for Oral Drug Delivery: Loading and Release of Five Model Drugs. *J. Control. Release* **2005**, *108*, 362–374.
25. Kilpeläinen, M.; Mönkare, J.; Vlasova, M. A.; Riikonen, J.; Lehto, V. P.; Salonen, J.; Järvinen, K.; Herzig, K. H. Nanostructured Porous Silicon Microparticles Enable Sustained Peptide (Melanotan II) Delivery. *Eur. J. Pharm. Biopharm.* **2011**, *77*, 20–25.
26. Kovalainen, M.; Mönkare, J.; Mäkilä, E.; Salonen, J.; Lehto, V. P.; Herzig, K. H.; Järvinen, K. Mesoporous Silicon (PSi) for Sustained Peptide Delivery: Effect of PSi Microparticle Surface Chemistry on Peptide YY3-36 Release. *Pharm. Res.* **2012**, *29*, 837–846.
27. Prestidge, C. A.; Barnes, T. J.; Mierczynska-Vasilev, A.; Skinner, W.; Peddie, F.; Barnett, C. Loading and Release of a Model Protein from Porous Silicon Powders. *Phys. Status Solidi A* **2007**, *204*, 3361–3366.
28. Tanaka, T.; Mangala, L. S.; Vivas-Mejia, P. E.; Nieves-Alicea, R.; Mann, A. P.; Mora, E.; Han, H. D.; Shahzad, M. M. K.; Liu, X. W.; Bhavane, R.; *et al*. Sustained Small Interfering RNA Delivery by Mesoporous Silicon Particles. *Cancer Res.* **2010**, *70*, 3687–3696.
29. Bimbo, L. M.; Mäkilä, E.; Raula, J.; Laaksonen, T.; Laaksonen, P.; Strommer, K.; Kauppinen, E. I.; Salonen, J.; Linder, M. B.; Hirvonen, J.; *et al*. Functional Hydrophobin-Coating of Thermally Hydrocarbonized Porous Silicon Microparticles. *Biomaterials* **2011**, *32*, 9089–9099.
30. Bimbo, L. M.; Sarparanta, M.; Mäkilä, E.; Laaksonen, T.; Laaksonen, P.; Salonen, J.; Linder, M. B.; Hirvonen, J.; Airaksinen, A. J.; Santos, H. A. Cellular Interactions of Surface Modified Nanoporous Silicon Particles. *Nanoscale* **2012**, *4*, 3184–3192.
31. Sarparanta, M. P.; Bimbo, L. M.; Mäkilä, E. M.; Salonen, J. J.; Laaksonen, P. H.; Helariutta, A. M.; Linder, M. B.; Hirvonen, J. T.; Laaksonen, T. J.; Santos, H. A.; *et al*. The Mucoadhesive and Gastroretentive Properties of Hydrophobin-Coated Porous Silicon Nanoparticle Oral Drug Delivery Systems. *Biomaterials* **2012**, *33*, 3353–3362.
32. Liu, D.; Mäkilä, E.; Zhang, H.; Herranz, B.; Kaasalainen, M.; Kinnari, P.; Salonen, J.; Hirvonen, J.; Santos, H. A. Nanostructured Porous Silicon-Solid Lipid Nanocomposite: Towards Enhanced Cytocompatibility and Stability, Reduced Cellular Association, and Prolonged Drug Release. *Adv. Funct. Mater.* **2013**, *23*, 1893–1902.
33. Sarparanta, M.; Bimbo, L. M.; Rytkönen, J.; Mäkilä, E.; Laaksonen, T. J.; Laaksonen, P.; Nyman, M.; Salonen, J.; Linder, M. B.; Hirvonen, J.; *et al*. Intravenous Delivery of Hydrophobin-Functionalized Porous Silicon Nanoparticles: Stability, Plasma Protein Adsorption and Biodistribution. *Mol. Pharm.* **2012**, *9*, 654–663.
34. Schwartz, M. P.; Yu, C.; Alvarez, S. D.; Migliori, B.; Godin, D.; Chao, L.; Sailor, M. J. Using an Oxidized Porous Silicon Interferometer for Determination of Relative Protein Binding Affinity through Non-Covalent Capture Probe Immobilization. *Phys. Status Solidi A* **2007**, *204*, 1444–1448.
35. Riikonen, J.; Mäkilä, E.; Salonen, J.; Lehto, V. P. Determination of the Physical State of Drug Molecules in Mesoporous Silicon with Different Surface Chemistries. *Langmuir* **2009**, *25*, 6137–6142.

36. Anderson, S. H. C.; Elliott, H.; Wallis, D. J.; Canham, L. T.; Powell, J. J. Dissolution of Different Forms of Partially Porous Silicon Wafers under Simulated Physiological Conditions. *Phys. Status Solidi A* **2003**, *197*, 331–335.
37. Ott, S.; Wunderli-Allenspach, H. Effect of the Virostatic Norakin (Triperiden) on Influenza Virus Activities. *Antiviral Res.* **1994**, *24*, 37–42.
38. Perez, L.; Carrasco, L. Involvement of the Vacuolar H(+)-Atpase in Animal Virus Entry. *J. Gen. Virol.* **1994**, *75* (Pt 10), 2595–2606